Chapter 7
High-Precision Mass Measurements of Radionuclides with Penning Traps

Michael Block

Abstract The mass of an atom is directly related to the binding energy of all its constituents. Thus, it provides information about all the interactions inside the atom. High-precision mass measurements hence allow studies of fundamental interactions and are of great importance in many different fields in physics. The masses of radionuclides provide information on their stability and their structure and are therefore of particular interest for nuclear structure investigations and as input for nucleosynthesis models in nuclear astrophysics. Penning trap mass spectrometry provides masses of radionuclides with unprecedented accuracies on the order of 10^{-8} and can nowadays be applied even to nuclides with short half-lives and low production rates. Utilizing advanced ion manipulation techniques radionuclides from essentially all elements produced in a broad range of nuclear reactions can be accessed. In this chapter the standard procedures of on-line Penning trap mass spectrometry are introduced and some representative examples of recent mass measurements are given.

7.1 Importance of Masses of Radionuclides

The mass of an atom is one of its fundamental properties and contains information about all the interactions inside the atom. The atomic mass m of the atom is smaller than the sum of the masses of all its constituents. This difference is due to the binding energy $B(N, Z)$ of all its constituents that can be obtained from the relation

$$B(N, Z) = [Nm_n + Zm_p + Zm_e - m(Z, N)]c^2; \tag{7.1}$$

where N is the neutron number, Z is the atomic number, m_n is the mass of a neutron, m_p is the proton mass, and m_e is the electron mass. Since the binding energy of the

M. Block (✉)
Gesellschaft für Schwerionenforschung mbH, Planckstrasse 1, 64291 Darmstadt, Germany
e-mail: m.block@gsi.de

W. Quint and M. Vogel (eds.), *Fundamental Physics in Particle Traps*,
Springer Tracts in Modern Physics 256, DOI: 10.1007/978-3-642-45201-7_7,

electrons is much lower than the nuclear binding energy it does not play a significant role for nuclidic masses at the present uncertainty level that can be reached for radionuclides so that $B_{nucl} \approx B(N, Z)$.

Masses play an important role in several fields of physics ranging from astrophysics to tests of the Standard Model [1, 2]. Mass measurements on stable nuclides can nowadays be performed with relative uncertainties on the order of about 10^{-11} [3–5], an accuracy that is required for the determination of fundamental constants and for very sensitive tests of fundamental symmetries. For example, a high-precision comparison of the proton-to-antiproton-mass ratio [6] provides a sensitive test of the charge, parity, and time reversal (CPT) symmetry. High-precision mass measurements also support precise tests of the Standard Model via the unitarity of the Cabbibo-Kobayashi-Maskawa quark mixing matrix by studies of superallowed β decays [7].

Mass measurements of radionuclides are a powerful tool for nuclear physics since they provide information on the stability and the nuclear structure of the investigated nuclides. Structural effects are revealed by several indicators such as the nucleon separation energies [1, 2]. In this context masses are often expressed by the mass excess *ME* defined as

$$ME = [m(\text{in u}) - A]; \tag{7.2}$$

where $A = N + Z$ is the mass number and the atomic mass unit u is defined as 1/12th of the mass of ^{12}C. A moderate precision on the order of 100 keV already allows identifying global structure phenomena such as major shell closures. For the investigation of nucleon pairing or deformation a higher precision on the order of 10 keV is often required. For tests of relations such as the isobaric multiplet mass equation (IMME) [8] even a higher precision on the level of about 1 keV is desirable. The IMME relation describes the masses of nuclides within an isobaric multiplet. It is based on the fact the strong interaction is approximately charge independent, a symmetry of this interaction that was already realized by Heisenberg [9] and Wigner [10] leading to the introduction of the isospin concept.

For nuclear structure studies it is important to reach radionuclides far away from stability whose proton-to-neutron ratio is very different from nuclides close to stability. Such extreme ratios often lead to changes in the structure and to new discoveries. It has been observed for example that the shell closure at $N = 28$ established in nuclides close to stability erodes in more neutron-rich nuclides [11]. The shell structure evolution can be tracked by masses.

A prominent nuclear structure phenomenon observed in light nuclides are halo structures. In such cases one or two nucleons are very loosely bound giving rise to exceptional large radii. For example, the two-neutron halo nucleus ^{11}Li [12] has a similar size as the much heavier nucleus ^{208}Pb illustrated also by mean square charge radii of ^{11}Li obtained by laser spectroscopy [13]. Halo candidate nuclides can be identified by mass measurements that reveal the neutron binding energy.

Another peculiar example are 'superheavy' elements ($Z \geq 104$) that are predicted to inhabit an 'island of stability' [14]. Their nuclei owe their very existence to nuclear shell effects that stabilize them against the disintegration by spontaneous fission

due to the strong Coulomb repulsion. The strength of these shell effects can be experimentally determined by direct mass measurements with Penning traps [15].

In general the proton and neutron separation (binding) energies determine the limits of stability given by the drip lines ($S_p(N,Z)$, $S_n(N,Z) = 0$) [16]. Since mass differences also determine the energy available for radioactive decays mass measurements allow identifying nuclides that exhibit exotic decay modes as for instance two-proton decay [17] or cluster radioactivity [18].

Masses and mass differences (Q values) also play an important role in nuclear astrophysics for the modelling of the formation of elements in stellar and explosive burning scenarios [19]. They determine the pathway of the different nucleosynthesis processes such as the rapid proton capture, the slow neutron capture and the rapid neutron capture process [20–22].

Accurate Q values are moreover relevant for neutrino physics. The search for rare processes such as neutrino-less double β decay and neutrino-less double electron capture needs very accurate Q values [23, 24]. The observation of one of these rare neutrino-less decay modes would unambiguously establish the neutrino as a Majorana particle and allow us to to determine the (anti)neutrino mass. The determination of the neutrino mass from the endpoint of the β decay spectrum of tritium as planned in the KATRIN experiment [25] for example, requires the very accurate knowledge of the ^{3}H-^{3}He mass difference.

The present knowledge on the masses of all about 3,500 nuclides known to date is summarized in the latest Atomic-Mass Evaluation (AME 2012) [26]. It contains all experimental data related to nuclidic masses obtained by different mass spectrometry techniques.

7.2 Mass Measurements at On-line Facilities

The development of mass spectrometry goes along with some important discoveries in physics. The 'birth' of mass spectrometry dates back to the time around 1900, a very productive period in physics with several ground breaking discoveries. A brief history on mass measurements and their evaluation can be found in an article by Audi [27].

An important milestone was the discovery of the electron by J. J. Thompson in 1897 that was based on a measurement of its mass-to-charge ratio [28], the same principle still applied in Penning trap mass spectrometry (PTMS) to date. Another important discovery was made 100 years ago by the observation of different neon isotopes using a mass spectrograph with electric and magnetic fields by the very same J. J. Thompson [29–32] who was awarded the Nobel prize in physics in 1906. F. W. Aston, J. J. Thompson's student, improved the mass spectrograph, where the different ions were registered on a photo plate, and discovered several new nuclides [33]. He was awarded the Nobel prize in chemistry in 1922. Further people involved in the development and improvement of mass spectrometers with higher resolution include for example Dempster [34], Mattauch and Herzog [35], Bainbridge, and Jordan [33].

Such devices reached a relative mass uncertainty of up to 10^{-5} and were used for a number of mass measurements of stable nuclides. Besides the discovery of multiple nuclides it led to the experimental observation of the mass defect, i.e. the difference between the atomic mass and the sum of the masses of its constituents as discussed in the introduction.

Mass measurements of radionuclides had to be carried out on-line at radioactive beam facilities. This endeavour started in the 1970s [36] at ISOLDE [37], the isotope separator on-line at CERN Geneva, and were initially performed by conventional mass spectrometers. However, such spectrometers reach their limits in applications to radionuclides due to the limited yield of such particles since in conventional mass spectrometers, for example of Mattauch-Herzog type, a high resolution often requires the use of narrow slits that reduces the transmission.

The advantage of a mass determination based on a cyclotron frequency measurement was realized by L. Smith who constructed an radiofrequency (rf) mass spectrometer in the 1960s [38] that could reach a higher precision. The 'Mistral' spectrometer installed at ISOLDE was a mass spectrometer of Smith type that was used in particular for measurements of light halo nuclides [39, 40]. However, its operation was rather complicated and the efficiency was limited so that this spectrometer was later decommissioned.

High-precision mass measurements of radionuclides in a Penning trap were pioneered almost thirty years ago, again at ISOLDE. The first mass measurement in a Penning trap was performed a couple of years earlier [41]. The installation of the Penning trap mass spectrometer ISOLTRAP [42, 43] marked the beginning of a new era in mass spectrometry.

Penning traps provide masses of radionuclides with unprecedented accuracies based on a direct cyclotron frequency measurement. Relative uncertainties on the order of 10^{-8} are nowadays feasible [1] and even radionuclides with short half-life [44] and low production rates [15] are accessible. For certain radionuclides even an accuracy of a few parts in 10^9 was already reported [45]. Since the installation of ISOLTRAP the landscape at radioactive beam facilities has changed dramatically. Today many Penning trap mass spectrometers are operated or planned at facilities around the world [43, 46–53]. The different devices show a large complementarity utilizing different production and measurement schemes in order to access practically the full nuclear chart.

A different technique for mass measurements that is also well suited for the application to radionuclides is time-of-flight mass spectrometry (ToFMS). First devices were used by A.E. Cameron and and D.F. Eggers around 1950 [54]. ToFMS can reach radionuclides far away from stability. However, the precision using conventional devices was typically only on the order of 10^{-6} for a reasonable flight path. This is often not sufficient to resolve nuclear isomers, and even nuclear isobars is some cases, and renders an accurate mass determination difficult. Recently new devices have been developed for ToFMS that allow a longer flight path of the ions of interest to achieve a higher resolving power maintaining a compact design. In so-called multi-reflection time-of-flight mass spectrometers [55–57] ion bunches are reflected multiple times between electrostatic mirrors. Such devices can reach a mass

resolving power of up to about 200,000 for a several turns within a few milliseconds cycle time. They are thus attractive as isobar separators [58] and may be used for mass measurements of very short-lived radionuclides with reasonable precision.

Another workaround in ToFMs is the use of a high-energy storage ring such as the experiment storage ring (ESR) at GSI Darmstadt [59]. An ion circulates in the ring with about 100 m circumference with a typical frequency on the order of MHz. In the so-called isochronous mode the mass of short-lived nuclides with microsecond half-lives can be determined by ToFMS with a precision of about 10^{-6} [60, 61]. Alternatively the Schottky mode, where even single ions can be detected electronically by the signal they induce into pick up electrodes while they orbit, mass measurements with a precision of about 10^{-7} can be obtained. However, the latter technique requires (electron) cooling of the radioactive ions so that only nuclides with half-lives of more than about one second can be tackled [60].

7.3 Penning-Trap Mass Spectrometry

Penning-trap mass spectrometry (PTMS) has in recent years developed into an elite method for high-precision mass measurements not only of stable nuclides but also for radionuclides [1]. This has opened up many new possibilities for studies related to various fields in physics as discussed in Sect. 7.1. With respect to nuclear structure investigations and to nuclear astrophysics it is necessary to extend the reach to exotic nuclides far away from stability. To this end, the introduction of buffer-gas stopping of ion beams along with advanced ion-manipulation techniques has been crucial. Nowadays PTMS can be applied to radioisotopes of essentially all elements, even of the elements above fermium, are meanwhile accessible to PTMS (c.f. Sect. 7.5.4). In the following the basic principles and some of the standard methods in PTMS are briefly introduced. Many of the general aspects discussed here also apply to PTMS of stable nuclides, however the focus here is on techniques relevant for experiments with radionuclides, where one has to deal with the challenges related to short half-lives and low production rates.

7.4 Production of Radionuclides at On-line Facilities

For the production and separation of radioactive ion beams a variety of techniques has been developed. The most important methods at accelerator facilities are presently the so-called ISOL method [62] and the in-flight technique. In ISOL facilities radionuclides are produced by fission and spallation reactions, typically induced by high-energy protons or light ions impinging on a thick target of a few mg/cm^2, for example made of uranium carbide. Alternatively neutron-induced fission or photo-fission are utilized. The radioactive ions are stopped in the target, diffuse out of the hot target cavity to the ion source where the radioactive atoms or molecules are

ionized by different methods and extracted as an ion beam at energies of typically 30–60 keV.

In addition to surface ionization nowadays more selective ionization methods such as laser resonant ionization are more and more often used to provide radioactive ion beams of higher purity [63]. The ion beam is mass separated in a magnetic separator, typically with a mass resoling power of about $m/\delta m \approx 3{,}000$ sufficient to separate isotopes, and delivered to the experiments. Since the diffusion out of the hot cavity takes time the access to very short-lived nuclides with half-lives below a few milliseconds is not feasible. Moreover, certain elements are not available due to their chemical properties. For example refractory elements cannot be produced at ISOL facilities.

The first ISOL facility, the the LISOL facility in Louvain-la-neuve [64], came into operation in 1989. The major ISOL facilities operated today are ISOLDE at CERN, Geneva [37], the ISAC facility at TRIUMF, Vancouver [65], and SPIRAL at GANIL, Caen [66]. The ion guide isotope separator on line (IGISOL) method [67] is a variant of the ISOL technique that overcomes some of its limitations. In the IGISOL technique the reaction target is installed in a buffer gas-filled chamber. Ions that recoil out of the target are slowed down in the gas and swept out by the gas flow through an extraction hole. The ion source system is kept at high voltage, typically about 30 keV, and the extracted ion beam is also mass separated by a magnetic separator prior to the distribution to the experiments. The IGISOL facility at Jyvaeskylae [68] is a user facility where this approach is applied.

In order to get access to all elements and to increase the reach to more exotic, short-lived radionuclides other production schemes have to be employed. The fragmentation of relativistic projectiles in combination with the in-flight separation by electromagnetic fragment separators gives access to all elements lighter than the projectile, i.e. in the case of uranium fragmentation isotopes of all elements up to uranium can be produced. This method requires projectile energies of about 100 *A*MeV to about 1 *A*GeV and can use thick targets of a few mg/cm^2. The beam quality (emittance) is worse than at ISOL facilities but rather pure beams can be obtained by two-stage separators. In addition to fragmentation also in-flight fission of fragments is utilized, an approach that is favourable for the production of neutron-rich nuclides. Facilities based on projectile fragmentation in operation comprise the radioactive isotope beam factory (RIBF) [69] at RIKEN, Wako-shi, Japan, the fragment separator (FRS) [70] at GSI in Darmstadt, Germany, and the A1900 [71] at the NSCL at Michigan State University, East Lansing, USA.

Another approach for the production of radionuclides is via fusion-evaporation reactions. Light to heavy-ion beams with energies around the Coulomb barrier, i.e. about 5 *A*MeV, are reacted with thin targets of about 0.5 mg/cm^2 to form a compound nucleus. The compound nucleus de-excites by the evaporation of protons, neutrons, or α particles depending on its excitation energy. The evaporation residue recoils out of the target and is separated from the primary beam by kinematic separators in flight. Either vacuum separators such as the velocity filter SHIP at GSI Darmstadt [72], Vassilissa at Dubna [73], or gas-filled separators such as the DGFRS in Dubna, Russia [74], the BGS at LBNL Berkeley, USA [75], GARIS at RIKEN

[76], RITU at Jyvaeskylae [77], or TASCA [78] at GSI Darmstadt are employed. These separators are optimized for high transmission and a high primary beam rejection but do generally not contain a separation based on the mass-to-charge ratio of the reaction products. This production scheme is presently the only way to access the heaviest elements. Using beams of stable nuclides and various targets including radioactive actinides targets this approach has been used for production of elements up to $Z = 118$ [74]. However, in general neutron-deficient nuclides are produced by this method.

7.4.1 Typical Layout of a Penning Trap Mass Spectrometer

The typical layout of an on-line Penning trap mass spectrometer setup for high-precision mass measurements of radionuclides is schematically depicted in Fig. 7.1. The initial stage has to be adapted to the properties of the radioactive ion beams delivered from a radioactive beam facility. The ion beams delivered by isotope separator online (ISOL) facilities have a moderate beam energy of 30–60 keV and a relatively good beam quality. Radioactive beams from in-flight separators have a much higher energy of tens of MeV up to hundreds of MeV per nucleon and a rather high emittance. Then buffer gas cells have to be employed for the conversion into a low-energy ion beam.

Independent of the production scheme one has to deal with low production rates that require highly efficient setups and sensitive diagnostics. The first beam preparation stage that is nowadays included in practically all state-of-the-art Penning trap mass spectrometers is a buffer-gas filled radiofrequency quadrupole (RFQ) cooler and buncher. In such buffer gas-filled linear Paul traps ions can be cooled by an inert buffer gas in a few milliseconds, accumulated over several cycles, and bunched. Thereby low emittance bunched ions beams can be prepared for an efficient injection into Penning trap systems. In this way also the properties of the ion beam are decoupled from the production stage.

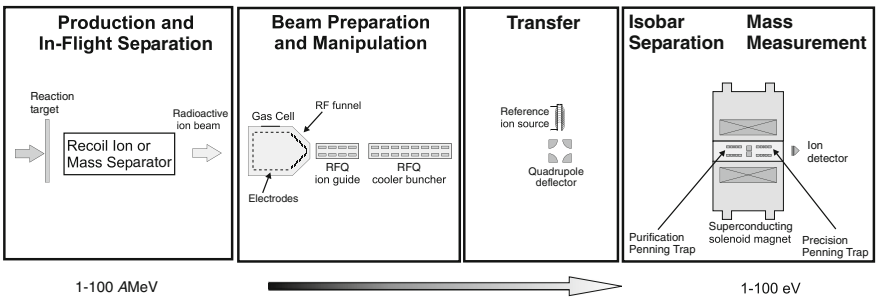

Fig. 7.1 Typical Layout of a Penning Trap Mass Spectrometer at an accelerator facility

In nuclear reactions often several nuclides are produced at the same time. In addition, contaminant ions may be created in the different beam preparation stages, for example by charge exchange reactions in the buffer gas, due the formation of molecular ions, or by background ions arising from nuclear decay products and unwanted ionization. The presence of unwanted ions that may even be much more abundant than the ion of interest has to be handled. The preparation of pure samples is crucial for high-precision mass measurements. To this end, in many setups a second Penning trap is utilized as a purification trap. In this trap a mass-selective buffer gas cooling and centering technique [79] is employed. This universal technique is suitable for radionuclides and provides a high mass resolving power of about 100,000 so that the separation of nuclear isobars can be accomplished. Alternatively other isobar separators such as magnetic separators [80] or multi-reflection time-of-flight mass spectrometer can be utilized [58]. The actual cyclotron frequency measurement is performed in the measurement trap, a precision Penning trap where the ions of interest are stored and manipulated in ultrahigh vacuum conditions. In the following the production of radionuclides is briefly addressed and the individual stages of an on-line Penning trap mass spectrometer are discussed in more detail.

7.5 Beam Preparation

The kinetic energy of the radionuclides produced by either of the techniques discussed above is too high for ion trapping. Thus, the ions have to be slowed down and prepared for the injection into a Penning trap first. In the case of an ISOL facility this can be accomplished utilizing an RFQ cooler buncher operated at high voltage [81]. The development of RFQ cooler-buncher devices was crucial to boost the performance of on-line Penning trap mass spectrometers and has made them a standard component for the preparation for low-energy radioactive beams. They are addressed in more detail in the next section.

Due to their much higher kinetic energy, about 50 MeV for fusion products up to several 100 *A*MeV for projectile fragments, the reaction products from in-flight separation cannot be slowed down electrostatically. An additional beam preparation stage in this case is provided by so-called buffer gas cells or ion-catcher devices [82–86] that are based on the IGISOL approach. In such gas cells the ions are slowed down in an inert buffer gas, typically helium, after passing a solid degrader that takes away most of the initial kinetic energy. The gas cells are operated at pressures on the order of 100 mbar for fusion products to about 1 bar for fragment beams. The ions remain singly or doubly charged in this process depending on their ionization potential and the cleanliness of the system. The ions are extracted by a combination of electric fields and buffer gas flow through an extraction hole, often a de Laval nozzle, within a few milliseconds at low pressure up to some hundred milliseconds at high pressure. In addition, cone-shaped electrode stacks [82, 85], so-called funnels, or ‘rf carpets’ [83, 87, 88] are utilized to facilitate an efficient extraction. In these devices a repelling force is created by an appropriate rf field to minimize ion losses during

the focussing on the extraction hole. The typical efficiency of gas stopping cells is presently about 10 % [82–85]. Since for every incoming ion up to 10^6 helium ion electron pairs are created a very high cleanliness and high gas purity are essential to avoid losses by charge exchange and molecule formation. Thus, cryogenic gas cells have recently been developed [88, 89] that will be operated at temperatures of 40–80 K so that most impurities freeze out. They are expected to boost the efficiency of gas stopping systems and provide purer beams. A so-called 'cyclotron gas stopper' [90, 91] has been suggested to handle radioactive beams with high rates. In this device the ions are also slowed down in a buffer gas in a weak focussing field of a cyclotron-type magnet that results in a spiraling motion that extends the ions' pathway. Such a device can be operated at a lower pressure and may be beneficial for the stopping of light particles. A prototype of a cyclotron gas stopper is being constructed at the NSCL [92].

7.5.1 Beam Preparation with an RFQ Cooler and Buncher

RFQ ion-beam cooler and buncher devices allow the preparation of low-energy rare isotope beams with high beam quality [46, 93–95]. Their main benefits are

- a reduction of the transversal emittance and the energy spread of the injected beam
- the beam properties of the extracted beam are decoupled from the beam properties of the injected beam
- ion accumulation over several accelerator cycles becomes possible
- bunched beams with variable repetition rate can be provided.

This is a prerequisite for many precision experiments on radionuclides. It allows an efficient injection of rare isotope beams into ion traps and improves the sensitivity of laser spectroscopy experiments. In this section the basic principle of an RFQ cooler-buncher is briefly summarized. More detailed information about RFQs and Paul traps can be found in various textbooks and monographs [96–99].

An RFQ cooler-buncher is a buffer-gas filled linear Paul trap [100] where the ions are confined in a quadrupolar time varying potential of the form

$$\phi(x, y, t) = \frac{V_0 \cos \Omega t}{r_0^2}(x^2 - y^2) \tag{7.3}$$

that is created by an rf voltage

$$U(t) = V_0 \cos \Omega t \tag{7.4}$$

applied to pairs of opposite electrodes of a four-rod structure as shown in Fig. 7.2. In contrast to the original mass filter design by Paul [100] nowadays mostly cylindrical electrodes are used instead of hyperbolic-shaped ones as they are easier to machine and the potential sensed by the ions close to the symmetry axis of the RFQ is similar.

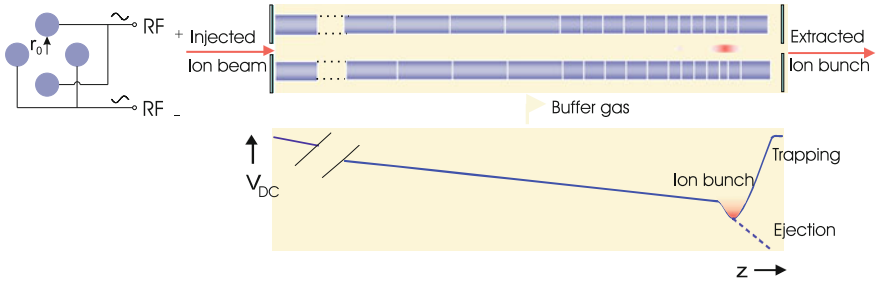

Fig. 7.2 Schematic view of an RFQ ion beam cooler and buncher. (*Top, left*) Cut in the transversal plane showing the connection of the rf voltage to the electrode rods. (*Top, right*) Cut of along the beam axis. The axially segmented buffer gas-filled electrode structure is shown. (*Bottom*) Axial DC potential in bunch mode

The ion motion can be described by Mathieu-type equations of motion of the form

$$\frac{\delta^2 u}{\delta^2 \xi} = (a - 2q\cos(2\Omega t))u = 0. \tag{7.5}$$

with generalized coordinates u and a parameterized time ξ. The Mathieu parameters a and q represent the DC and rf amplitudes of the trapping potential, respectively.

$$a = \frac{4eU_0}{mr_0^2\Omega^2} \tag{7.6}$$

$$q = \frac{2eU_0}{mr_0^2\Omega^2}, \tag{7.7}$$

Stable solutions of the Mathieu equation are obtained for certain values of a and q. The stability criterion can be depicted in a diagram as shown in Fig. 7.3 where a stable confinement is achieved choosing operating parameters within the shaded region. For an RFQ ion-beam cooler-buncher typically $a = 0$ is chosen leading to the stability condition $q < 0.908$ [98]. From this condition the required rf amplitude for a selected operation frequency Ω and a given charge-to-mass ratio can be derived. The motion in the rf potential can also be described in terms of a time-averaged pseudo-potential as introduced by Dehmelt [101]. The ion motion

$$x(t) = \{x_0\cos(\omega t)\}\cos\Omega t \tag{7.8}$$

is a composition of a forced oscillation following the driving rf field resulting in a so-called micro-motion at frequency Ω and a harmonic oscillation, the macro-motion, at a frequency

$$\omega = \frac{q}{\sqrt{8}}\Omega. \tag{7.9}$$

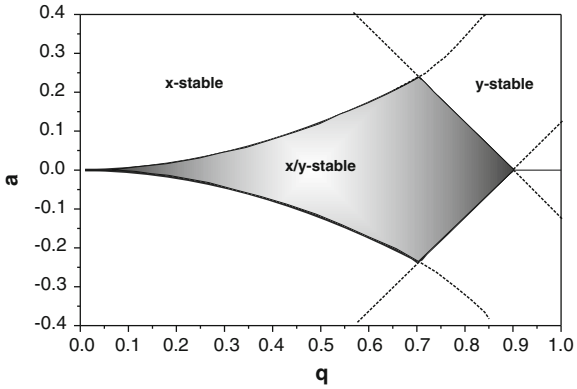

Fig. 7.3 Stability diagram of an rf trap. A stable confinement is achieved for operating points (a_o, q_o) within the *shaded* region

For typical parameters of an RFQ ion-beam cooler of $a = 0$, $q \approx 0.4$, and $\Omega = 1$ MHz an oscillation frequency of $\omega = 2\pi \cdot 76$ kHz is obtained for an ion with mass $A = 100$.

While the radial confinement in the RFQ is provided by an rf field as discussed above a static electric field gradient is superimposed for the axial confinement and to drag the ions through the buffer gas into a potential well at the end of the RFQ. To this end the electrode rods are segmented so that the desired axial field gradient can be created as indicated in Fig. 7.2. The RFQ is filled with a light inert buffer gas, typically high-purity helium, at a pressure of about 10^{-3} mbar so that the ions are thermalized in collisions with the buffer gas atoms within a few milliseconds. If the RFQ is operated as ion guide in transmission mode a higher pressure is typically used since the ions have to be cooled in a single pass, whereas a lower pressure is favourable for bunching. This buffer gas cooling technique is universal and thus suitable for radioactive ions. It can be applied as long as the mass of the buffer gas atoms is small compared to the mass of the ion to be cooled. The application of buffer gas cooling results in an emittance reduction of an injected ion beam to about $10\,\pi$ mm×mrad or less and results in a longitudinal energy spread of less than 1 eV. The cooled ions can be accumulated in a potential well at the end of the rod structure where they form an ion bunch. An ion bunch is extracted by switching the voltages applied to the end electrodes of the RFQ. A typical bunch width of about 100 ns–1 μs is achieved. The bunch properties can be influenced by the trapping potential and the extraction voltages. There are several designs in use for RFQ cooler bunchers, in some of which the electrodes for the DC potential are separated from the rf electrodes [95].

7.5.2 Penning Traps

Penning traps are well described in the literature in several review articles, monographs, and textbooks [96, 97, 99, 102, 103]. The application of Penning traps for high-precision mass spectrometry has also been addressed in various works [1, 104, 105]. In this section the basics are briefly summarized and the relevant methods with respect to PTMS of radionuclides are introduced.

The concept of a Penning trap goes back to the works of F. Penning, who actually worked on more accurate pressure gauges but was credited with the name nonetheless [106], and Pierce [107]. However, the real breakthrough using Penning traps for high-precision experiments was related to Dehmelt's famous experiment on the anomalous magnetic moment of a free electron [101]. This ingenious experiment earned him the the Nobel prize in physics in 1989 together with Wolfgang Paul, another ion trap pioneer introducing the RF trap nowadays referred to as Paul trap, and Norman Ramsey, whose method of separate oscillatory fields has meanwhile also found its way into PTMS [108].

In a Penning trap a charged particle is confined by a strong homogeneous magnetic field $\mathbf{B} = B_0\mathbf{z}$ and a superimposed electrostatic quadrupolar field $\mathbf{E}$ created by a set of electrodes as shown in Fig. 7.4. A quadrupolar potential of the form

$$U(\rho, z) = \frac{U_0}{\rho_0^2 + 2z_0^2}(\rho^2 - 2z^2), \tag{7.10}$$

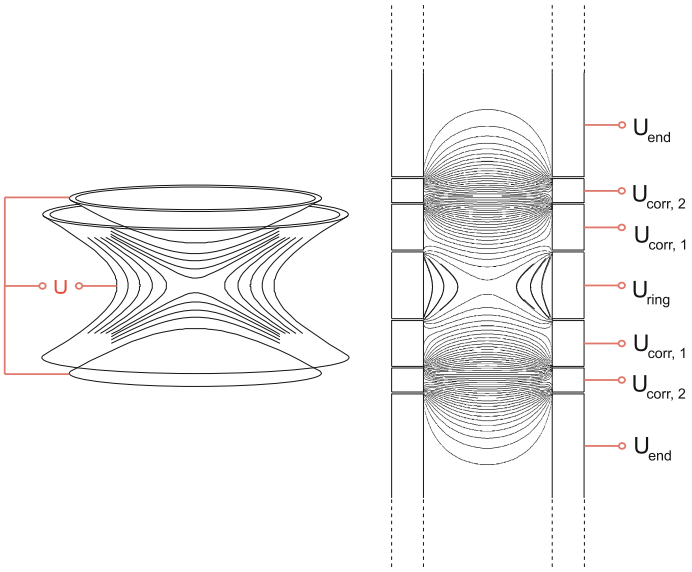

Fig. 7.4 Ideal Penning trap with hyperbolical electrodes (*left*) and the motion of a single ion in the trap (*right*)

where ρ_0 and z_0 are the trap dimensions as shown in Fig. 7.4, is created applying a voltage U between a ring electrode and two endcap electrodes of the trap. In practice traps with hyperbolic electrodes as well as with cylindrical electrodes are in use. With the characteristic dimension d

$$\rho_0^2 + 2z_0^2 = 4d^2 \tag{7.11}$$

the potential can be rewritten as

$$U(\rho, z) = \frac{U_0}{4d^2}(\rho^2 - 2z^2). \tag{7.12}$$

Solving the equations of motion for a single trapped ion leads to three independent eigenmotions: A harmonic oscillation in axial direction at frequency

$$\omega_z = \sqrt{\frac{qU}{md^2}} \tag{7.13}$$

and two radial motions, the cyclotron motion at the modified cyclotron frequency

$$\omega_+ = \frac{\omega_c}{2} + \sqrt{\frac{\omega_c^2}{4} - \frac{\omega_z^2}{2}} \tag{7.14}$$

and the magnetron motion at a frequency

$$\omega_- = \frac{\omega_c}{2} - \sqrt{\frac{\omega_c^2}{4} - \frac{\omega_z^2}{2}}. \tag{7.15}$$

The magnetron frequency is to first order independent of the mass of the stored ion. For typical parameters the hierarchy of the eigenfrequencies is $\omega_- < \omega_z < \omega_+$. In a Penning trap even single ions can be confined under well-defined, almost perturbation-free conditions in ultrahigh vacuum. This results in long observation times, in the case of radionuclides ultimately limited by the half-life, that lay the ground for experiments of unprecedented precision.

The mass m of an ions with charge q can be obtained from its free cyclotron frequency ω_c at which it orbits in a magnetic field of strength B.

$$\omega_c = 2\pi\nu_c = \frac{qB}{m}. \tag{7.16}$$

For PTMS in particular the following relations between the free cyclotron frequency and the eigenfrequencies in the trap are important:

$$\omega_c = \omega_+ + \omega_-; \tag{7.17}$$

$$\omega_z^2 = 2\omega_+\omega_-; \tag{7.18}$$

$$\omega_c = \omega_+\omega_- = \sqrt{\omega_+^2 + \omega_-^2 + \omega_z^2}; \tag{7.19}$$

where the latter relation is also known as the Brown-Gabrielse invariance theorem [102]. It is often used for the cyclotron frequency determination of stable nuclides. Equation 7.17 is typically employed for PTMS of radionuclides since ν_c can be measured directly using the so-called time-of-flight ion-cyclotron resonance (ToF-ICR) technique [109, 110]. This method is universal and fast and has become the method of choice for the cyclotron frequency measurement in on-line PTMS applications. A discussion on its applicability and limitations for high-precision PTMS in real Penning traps was recently presented by Gabrielse [111].

The basic principle of the ToF-ICR method is explained in the following. The ion's magnetron motion is excited by a dipolar rf field in the azimuthal plane of the Penning trap at the frequency ν_-. Thereby the ion, initially injected into the trap on axis, is prepared in a pure magnetron motion on a radius R_m. Subsequently a quadrupolar rf field at the frequency ν_{rf} is applied in the azimuthal plane. The frequency of this rf field is varied around the expected cyclotron frequency. If $\nu_{rf} = \nu_c$ the two radial motions are coupled and energy is transferred converting the magnetron motion into cyclotron motion. If the length and the amplitude of the rf pulse are chosen properly then the ion is prepared in a pure cyclotron motion with radius $R_c = R_m$ after the second excitation. This conversion is accompanied by an increase of the radial kinetic energy of the ion, i.e. the energy in the plane perpendicular to the magnetic field axis, giving rise to a resonance. This can be detected via the orbital magnetic moment $\boldsymbol{\mu_B}$ of the ion that increases on resonance. This change can be detected via the time of flight of the ion through the magnetic field gradient of the superconducting solenoid of the Penning trap to an ion detector outside the magnet field [109, 110]. In the magnetic field gradient the ion experiences an accelerating axial force

$$\mathbf{F} = \nabla \boldsymbol{\mu_B} \cdot \mathbf{B};, \tag{7.20}$$

so that resonantly excited ions reach the detector earlier than those off resonance. If the time of flight is recorded as a function of the excitation frequency ν_{rf} a resonance as shown in Fig. 7.5 is obtained. From a fit of the theoretically expected line shape [103, 110] to the resonance curve the cyclotron frequency is derived. In an ideal case the linewidth of such a time-of-flight cyclotron resonance is Fourier limited and thus approximately given as [104] $\delta\nu = 0.8 \cdot T_{RF}^{-1}$.

The resolving power $\Re$ of the ToF-ICR method scales according to

$$\Re = \frac{\nu}{\Delta\nu} = \frac{m}{\Delta m} \propto \nu_c T_{rf}. \tag{7.21}$$

It is proportional to the product of the excitation time T_{RF} and the cyclotron frequency. For radionuclides the excitation time is ultimately limited by the half-life

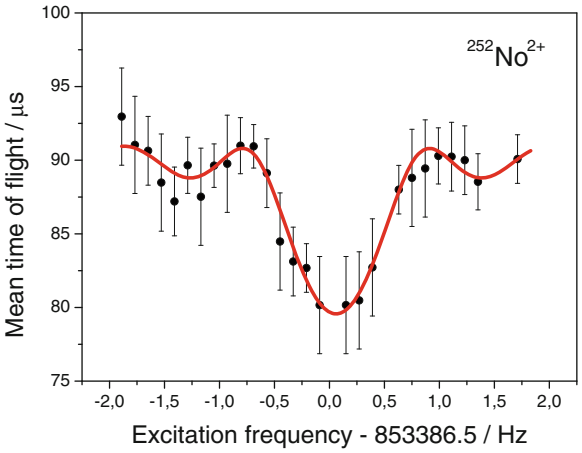

Fig. 7.5 Cyclotron resonance of ^{252}No adapted from [112]. The *line* represents a fit of the theoretically expected lineshape to the data points

of the investigated particle. An optimum is then reached for $T_{rf} \approx 3T_{1/2}$ [113]. The statistical uncertainty of the frequency determination is given by the relation [114]

$$\frac{\delta m}{m} \propto \frac{1}{\Re\sqrt{N_{det}}} \propto \frac{m}{qBT_{rf}\sqrt{N_{det}}} \tag{7.22}$$

where N_{det} is the number of detected ions after excitation and extraction from the trap. Typically at least about 30 ions have to be accumulated to obtain a resonance curve [15, 112]. In on-line PTMS the accuracy of cyclotron frequency measurements is often limited by statistics due to the low production rates of the radionuclides of interest. For an excitation time of 1 s a resolving power of about $R \approx 1{,}000{,}000$ can be reached for an ion of mass $A = 100$ in a magnetic field of $B = 7\ T$. The corresponding statistical uncertainty that can be reached for a nuclide with a half-life of about one second for a number of 1,000 detected ions is then $(\frac{\delta m}{m})_{stat} = 3 \times 10^{-8}$.

A higher accuracy can be obtained applying different excitation schemes to the ToF-ICR method such as an octupolar excitation [115–117] or a Ramsey-type excitation [108]. Alternatively highly charged ions can be utilized as recently demonstrated with the TITAN spectrometer at the TRIUMF facility in Vancouver [118]. Another approach that has recently been developed is the so-called phase sensitive PI-ICR method [119] where the ion motion is imaged onto a spatially resolving microchannel plate detector. Then the (radial) eigenfrequencies can be measured via a phase measurement. In this way one can overcome the Fourier limit of the ToF-ICR method. With SHIPTRAP a gain in resolving power by a factor of forty and a gain in precision by a factor of about five has already been demonstrated with this novel method [119]. This allows measurements with a high accuracy in rather short time and thus extends the reach of PTMS to shorter-lived nuclides.

7.5.3 Contributions to the Systematic Uncertainty in PTMS

For high-precision mass measurements in addition to the statistical uncertainty several systematic uncertainties have to be considered. The most relevant systematic effects for PTMS of radionuclides have been discussed for example by Bollen et al. [104] following an analysis for electrons by Brown and Gabrielse [102]. For a high-precision cyclotron frequency measurement the following effects can lead to cyclotron frequency shifts

- a deviation of the electric trapping field from a pure quadrupolar field
- spatial magnetic field inhomogeneities
- temporal fluctuations of the confining fields
- a tilt of the electrical field axis relative to the magnetic field axis
- ion-ion interaction if more than one ion is trapped at a time.

7.5.3.1 Temporal Magnetic Field Changes

The magnetic field strength B has to be known precisely in order to derive the mass with high precision from the measured cyclotron frequency according to Eq. 7.16. However, the magnetic field also changes in time. An intrinsic decay due to flux creep that is approximately linear over time on the order of 10^{-8}/h is accompanied by short-term fluctuations. These can arise for example from changes of parameters like the ambient temperature that lead to changes in the magnetic susceptibility of the materials inside the magnet bore and from changes of the pressure in the liquid helium cryostat of the solenoid, and thus the boiling point of the liquid helium. Moreover, external magnetic stray fields that are often unavoidable at accelerator facilities can play a role.

An example of the magnetic field stability is presented in Fig. 7.6 where the magnetic field evolution of the solenoid of the SHIPTRAP mass spectrometer is shown. The general trend shows a linear decay of the magnetic field over time with

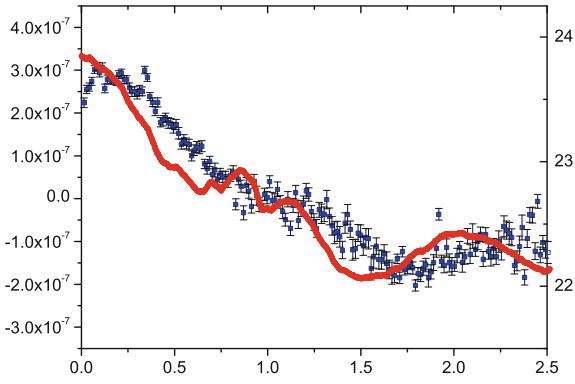

Fig. 7.6 Relative magnetic field changes in the SHIPTRAP solenoid over a period of 2.5 days. The magnetic field was monitored by cyclotron frequency measurements of $^{85}Rb^{+}$ ions. The *red line* represents the temperature in the bore of the superconducting solenoid

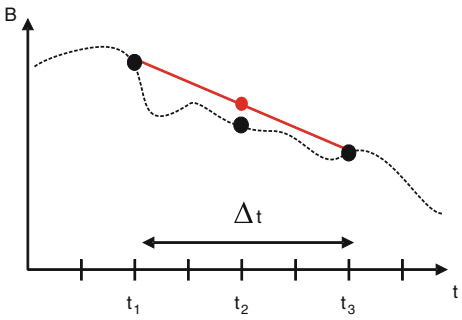

Fig. 7.7 Principle of the magnetic field calibration using a linear interpolation. The actual magnetic field is represented by the *dashed line*. The *black dots* marked the time where a calibration measurements is performed. The interpolation is indicated by the *full line*

superimposed fluctuations on shorter time scales. These are mainly correlated to changes of the temperature measured inside the bore of the solenoid.

The temporal fluctuations of the magnetic field are accounted for in PTMS by calibrating the magnetic field via a cyclotron frequency measurement of a reference ion with well-known mass that is chosen such that its mass-to-charge ratio is similar to that of the ion of interest. Then both ions are trapped at the same positions in the trap and sense the same field. Calibration measurements are then performed before (t_1) and after (t_3) the frequency measurement of the ion of interest at time t_2. The scheme is qualitatively illustrated in Fig. 7.7. From the measured cyclotron frequencies a linear extrapolation to the time of the actual measurement t_2 is performed providing the frequency $\nu_c^{ref}(t_2)$ according to the relation

$$\nu_c^{ref}(t_2) = \nu_c^{ref}(t_1) + \frac{\nu_c^{ref}(t_3) - \nu_c^{ref}(t_1)}{t_3 - t_1}(t_2 - t_1), \tag{7.23}$$

Thereby the linear decay of the magnetic field is corrected. The effect of nonlinear magnetic field fluctuations is considered by a systematic uncertainty that depends on the measurement time needed to acquire a single cyclotron resonance. This uncertainty due the difference between the actual magnetic field value and the interpolated values can be estimated experimentally by an analysis as described in [120]. In the example of SHIPTRAP mentioned above a time dependent uncertainty due to nonlinear magnetic field fluctuations was determined [121] to be on the order of

$$\sigma_B \approx 2 \times 10^{-9}/min \times \Delta t, \tag{7.24}$$

where Δt is the time interval between consecutive calibration measurements in minutes. This uncertainty is quadratically added to the statistical uncertainty of the frequency measurements. Since part of the temporal magnetic field fluctuations are due to changes of the temperature in the bore of the solenoid and the pressure in the liquid helium dewar of the solenoid an active stabilization system for both parameters can improve the long time stability of the magnetic field. At SHIPTRAP such a system has recently been implemented and reduced the uncertainty related to temporal

fluctuation of magnetic field to [122].

$$\sigma_{\omega_B} \approx 2 \times 10^{-11}/min \times \Delta t. \tag{7.25}$$

The primary result of a PTMS experiment following this calibration procedure is thus the frequency ratio r between the cyclotron frequencies of the ion of interest and the reference ion

$$r = \frac{\nu_c(t_2)}{\nu_{c,ref}(t_2)}. \tag{7.26}$$

The uncertainty δr of a measured frequency ratio r is comprised by the statistical uncertainty σ_{stat} and a systematic uncertainty σ_{syst} that includes for example the uncertainty due to nonlinear fluctuations of the magnetic field σ_B as discussed above

$$\delta r = \sqrt{\sigma_{stat}^2 + \sigma_{syst}^2} = \sqrt{\sigma_B^2 + \sigma_{stat}^2 + \sigma_{res}^2}, \tag{7.27}$$

and σ_{res} contains all other systematic uncertainties.

The atomic mass is obtained from the measured frequency ratio according to the following relation using the most recent and hence most accurate mass value of the reference ion m_{ref}

$$m = \frac{q}{q_{ref}} r(m_{ref} - q_{ref} m_e) + q m_e, \tag{7.28}$$

where m_e is the electron mass and q and q_{ref} are the charge states of the ion of interest and the reference ion. For the typical uncertainties achieved for radionuclides the binding energy of the electrons can be neglected. If carbon cluster ions are used as mass reference [120] absolute mass measurements can be performed since the atomic mass is defined via the mass of ^{12}C.

7.5.3.2 Spatial Homogeneity of the Confining Fields

The electric trapping potential of a real trap deviates from a pure quadrupole potential even for a hyperbolic electrode geometry due to several reasons, for example, machining imperfections, misalignments, the truncation of electrodes, and additional holes required for the injection and extraction of particles. The impact of such perturbations can be compensated to some extent by additional correction electrodes. In a similar way a harmonic trapping potential can be realized using a cylindrical trap geometry with open endcaps [123]. Cylindrical traps are simpler to machine and can be pumped more efficiently than traps with hyperbolic electrodes. In such a cylindrical trap a careful tuning of the trapping voltages (applied to the correction electrodes) is particularly important. In addition, patch potentials on the electrode surfaces can play a role. Those are generally avoided by gold plating of the electrodes.

In general a perfect harmonic potential is only realized in a small region around the trap center whereas for larger distances from the trap center higher order multipoles of the trapping field become significant. The deviation from the ideal quadrupole field thus also depends on the amplitude of the ion motion. Therefore the application of ion cooling to constrain the amplitudes of the ion motion to a region close to trap center is crucial for high precision measurements.

The deviation of the real trapping potential from a pure quadrupole is expressed by the coefficients C_i of a multipole expansion of the real potential ϕ_{real}:

$$\phi_{real} = \frac{U_0}{2} \sum_i C_i (\frac{r}{d})^i P_i(cos\theta) \tag{7.29}$$

For an ideal quadrupole potential $C_2 = -2$, while all other coefficients vanish. In real traps typically the next two higher order terms, the octupole (C_4) and dodecapole (C_6) term, play a role. As long as the radial symmetry is not broken all odd expansion coefficients vanish. The cyclotron frequency shift in case of non-vanishing C_4 and C_6 terms is given [102] by

$$\Delta\omega_c^{electr} = C_4 \frac{3}{4}(\rho_+^2 - \rho_-^2)\frac{\omega_z^2}{\omega_c^2} + \frac{15}{4}\frac{C_6}{d^2}[\rho_z^2(\rho_-^2 - \rho_+^2) - (\rho_-^4 - \rho_+^4)]. \tag{7.30}$$

It depends on the amplitudes of the ion motion but is approximately mass independent. The size of the different multipole coefficients can be estimated for a given electrode geometry by fitting Eq. 7.29 to the numerically calculated potential in a certain region around the trap center.

Besides electric field anharmonicities also spatial magnetic field inhomogeneities lead to frequency shifts. The intrinsic homogeneity of a commercially available state-of-the-art superconducting solenoid magnet is on the order of $\Delta B/B = 0.1 - 1$ ppm/cm^3 if no special measures are taken. The actual magnetic field B sensed by the trapped ions can be additionally modified by materials introduced into the magnetic field such as the trap electrodes or the trap vacuum tube due to a non-zero magnetic susceptibility. The modification of the magnetic field around the trap center can be described by

$$\frac{\delta B}{B_0} = \beta_2[(z^2 - \rho^2/2)z - z\rho], \tag{7.31}$$

where B_0 is the magnetic field at the trap center, and z and ρ are the motional amplitudes, since a linear term vanishes. The resulting cyclotron frequency shift is then given by [102]

$$\Delta\omega_c^{magn} = \omega_c\beta_2[z^2 - \frac{\rho_+^2}{4}(1 + \frac{\omega_c}{\omega_+ - \omega_-}) - \frac{\rho_-^2}{4}(1 + \frac{\omega_c}{\omega_+ - \omega_-})] \tag{7.32}$$

This shift is proportional to the cyclotron frequency and hence, depends on the mass of the ion. This effect can be minimized by using materials with low magnetic sus-

ceptibility for the trap construction and reducing the amount of material introduced. Moreover, the design should be such that the radial symmetry is maintained.

7.5.3.3 Trap Misalignments

Misalignments of the individual trap electrodes can be minimized by a careful mechanical trap design and thus do not play a significant role in particular for cylindrical traps. However, a misalignment of the electrical field axis with respect to the magnetic field axis is much harder to avoid in practice. A tilt of the axis by an angle θ results in a shift of the eigenfrequencies [104] by

$$\Delta\omega_c{}^{tilt} \approx \frac{9}{4}\omega_- \sin^2\theta, \tag{7.33}$$

where ω_- is the magnetron frequency. However, all eigenfrequencies shift in the same way. This shift is to first order mass independent. By a careful alignment of the trap in the magnet bore this tilt angle is minimized. Typical values that can be achieved are on the order of 1 mrad.

7.5.3.4 Ion-Ion Interactions

In experiments with radioactive particles contaminant ions can be created either in the production stage by unwanted nuclear reactions, in the ion preparation process, or by the radioactive decay of the investigated particle itself. The presence of of unwanted ions in the trap can result in a shift the cyclotron frequency due to the Coulomb interaction between different ions. In general this effect is avoided if a measurement is performed with only a single trapped ion at a time, however this is not always possible in on-line experiments. If the different ions in the trap have the same mass-to-charge ratio then the field acts on the center of mass and no frequency shift occurs. In the case of contaminant ions with different mass-to-charge ratio one resonance shifted in frequency is observed if the two different cyclotron frequencies cannot be resolved. If the mass difference of the ions is large enough that the individual resonances are resolved both resonances shift to lower frequencies and the frequency shift is proportional to the number of trapped ions [124]. Therefore, in a precision measurement possible frequency shifts are revealed by an analysis as described in [120]. In this method the cyclotron frequency is determined as a function of the number of ions in the trap at a time by dividing the data into subsets with similar statistics. Then the cyclotron frequency is linearly extrapolated to one ion in the trap taking into account the ion detection efficiency. Frequency shifts due to image charge effects do not play a role for radionuclides yet as they are typically two or three orders of magnitude smaller than the statistical uncertainty.

7.5.4 Applications of High-Precision Mass Measurements

In this section some recent examples of mass measurements of radionuclides performed by PTMS are given. They illustrate the versatility and the present performance of PTMS for radionuclides. The first example is related to mass measurements in the context of nuclear astrophysics. The second example addresses experiments in the region of the heaviest elements.

In the stellar nucleosynthesis of heavy elements in the universe various scenarios and processes are discussed. The slow and rapid neutron capture process (s and r process) are expected to be responsible for the creation of most of the heavy elements beyond iron [21, 22]. The rapid proton-capture process (rp process) is believed to be responsible for so-called X-ray bursts [20] and may also take place in a neutrino driven wind in core collapse supernovae [125]. Type I x-ray bursts can occur when a neutron star accretes matter from an expanded companion star and last for a few seconds. For a detailed astrophysical modelling of the various processes under different conditions several nuclear properties such as half-lives and masses are required input parameters. In order to eliminate or at least minimize the impact of nuclear physics-related uncertainties on the astrophysical conclusions accurate data of the relevant properties are needed for many, often very exotic, radionuclides.

The predicted pathway of the r process [21] proceeds in a region of very neutron-rich nuclides some of which will only be accessible at next generation radioactive beam facilities such as FAIR in Darmstadt [126], FRIB at Michigan State university [127], or SPIRAL 2 at GANIL [128].

The rp process consists of a sequence of proton capture reactions and subsequent beta decays in competition with photodisintegration. The predicted rp process pathway [20] reaches out to exotic nuclides at the proton drip line that can already be accessed for practically all nuclides relevant to the rp process at present radioactive beam facilities. However, some of them are short-lived and can only be produced in minute quantities. The impact of masses on the r and rp process was discussed in several articles [19, 129, 130]. In these investigations it was found that masses are required with an uncertainty on the order of 10 keV or below. For so-called 'waiting points' a higher precision is often needed.

Waiting points in the rp process are rather long-lived nuclides encountered when the proton capture reaches the drip line so that the process only proceeds towards heavier nuclei after the β decay of the waiting point nuclide (or if it can be bypassed via two-proton capture). Thus waiting point nuclides have a large impact on the characteristics of an x-ray burst, for example the corresponding light curve. Depending on the density and temperature conditions in the stellar environment the effective half-life of a waiting point, i.e. the time until the rp process proceeds, can be altered significantly. An example is shown in Fig. 7.8 for the waiting point ^{68}Se to illustrate the impact of precise mass values. The effective lifetime of ^{68}Se as a function of temperature was determined by a local network calculation based on mass measurements with LEBIT [131]. The effective lifetime previous to this experiment was 10.7(6.8) s so that ^{68}Se would not be a strong waiting point within the

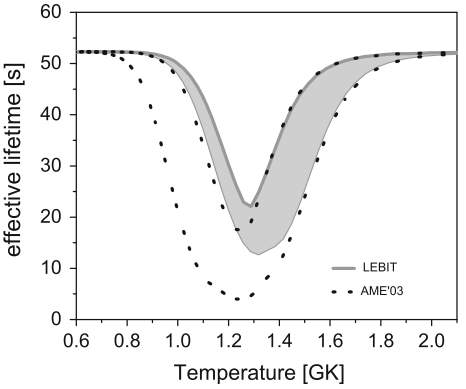

Fig. 7.8 Impact on the mass on the effective half-life of the rp process waiting point ^{68}Se (adapted from [131]) for different temperatures

experimental uncertainty. Based on the new accurate mass values a lifetime of 17.4(4.5) s was obtained indicating that ^{68}Se is indeed a strong waiting point for all relevant conditions.

In recent years the masses of many radionuclides relevant for nuclear astrophysics have have been measured with high accuracy by direct mass measurements using PTMS at various radioactive beam facilities [132–139]. In certain areas, for example around ^{84}Mo, the estimated masses have been found to deviate from the new data by as much as 1 MeV [135]. Based on the new data improved calculations were performed that contribute to a better understanding of nucleosynthesis.

An example for mass measurements in the context of nuclear structure studies is related to direct mass measurements of the heaviest elements. Superheavy nuclides owe their very existence to nuclear shell effects that stabilize them against the disintegration by spontaneous fission due to the strong Coulomb repulsion in nuclides with high-Z. The fission barrier calculated according to macroscopic nuclear models [14] vanishes for nuclides with $Z \approx 104$. However, a finite fission barrier is obtained for superheavy elements when including nuclear shell effects. Superheavy elements are predicted to inhabit an 'island of stability' by different theoretical models that, however, still disagree on the exact location an extension of this island. The predicted center is located at $Z = 114$, 120, or 126 and $N = 172$ or 184 depending on the parametrization [14, 140–142]. Experimentally this concept is supported by several new elements that have been discovered in recent years in different laboratories worldwide with the latest claims reaching up to element $Z = 118$ [72, 74, 143–147].

However, binding energies that are at the heart of superheavy nuclides have experimentally been out of reach for a long time. The transuranium nuclides have not been accessible by PTMS either due to their low production rates of due to to their production scheme that requires additional preparation steps. Isotopes of the elements above fermium ($Z = 100$) can only be produced by fusion-evaporation reactions with heavy-ion beams typically from ^{40}Ar to ^{70}Zn and either lead and bismuth targets or actinide targets from uranium to californium. However, the production rates are very low even for primary beam intensities of almost 10^{13} particles per second.

About four ions per second can be delivered to a PTMS setup for ^{254}No ($Z = 102$), but the rate drops steeply to about one atom per three days for element flerovium ($Z = 114$) [144]. The actual number of ions available for PTMS is even lower due to the losses during the slowing down and beam preparation procedures resulting in overall efficiencies on the order of a few percent. Such low rates are a major challenge for PTMS since they result in very long measurement times of a few days over which all relevant parameters such as the trapping fields have to be stable.

Nonetheless, recently direct mass measurements of several nobelium and lawrencium isotopes have been performed with the Penning trap mass spectrometer SHIPTRAP at GSI in Darmstadt, Germany [15, 112]. In case of the nuclide ^{256}Lr the yield was on the order of two particles per minute. For a cyclotron resonance about 50 ions were detected statistically distributed over a period of about four days. The masses have been determined with an accuracy of down to about 10 keV and now provide reliable anchor points in the region of the heaviest elements.

New elements in this region have so far been identified by the observation of α decay chains that connect new nuclides to well known nuclides. Prior to the SHIPTRAP experiments also the masses of nuclides in this region were determined in this way, i.e. indirectly from the measured α decay energy and the known mass of the daughter nuclide. However, this method works only well if the α decay occurs between nuclear ground states as for even-even nuclides, else it requires a detailed knowledge about the nuclear level scheme. In addition, the mass uncertainties accumulate going along the chain.

In addition to providing anchor points direct mass measurements allow mapping the strength of nuclear shell effects as demonstrated by SHIPTRAP [15]. From accurate experimental mass values the strength of the shell effects can be derived according to Eq. 7.34. The difference of several nuclidic masses provides the so-called shell gap parameter $\delta_{2n}(N, Z)$ that amplifies the visibility of a shell closure.

$$\delta_{2n}(N, Z) = S_{2n}(N, Z) - S_{2n}(N + 2, Z) \tag{7.34}$$

$$= 2ME(N, Z) + ME(N - 2, Z) + ME(N + 2, Z), \tag{7.35}$$

where $S_{2n}(N, Z)$ is the two-neutron separation energy. The binding energy of neighboring nuclides changes most significantly when a closed shell is reached since the nuclides are most strongly bound for closed shells. Such differences can also be visualized by the other mass differences such as the two-nucleon separation energy $S_{2n/2p}(N, Z)$. Since the pairing between nucleon results in a change of the binding energy that would result in an odd even staggering of one-nucleon separation energies two nucleon separation energies are used to visualize trends in the nuclear structure evolution.

Figure 7.9 shows the shell gap parameter for nobelium isotopes around neutron number $N = 152$. The effect of a closed neutron shell is clearly visible by the peak in $\delta_{2n}(N, Z)$. The strength of this shell closure in a region of deformed nuclei is much weaker though than for example in the spherical doubly magic nucleus ^{208}Pb where the shell gap is about 8 MeV large. The accurate experimental data provide a sensitive

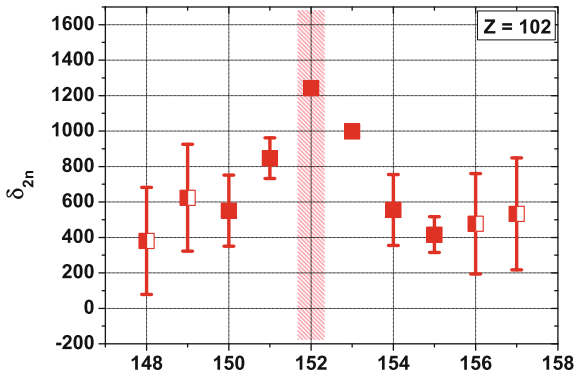

Fig. 7.9 Neutron shell gap for neutron numbers around $N = 152$ (adapted from [15]). Experimental data are given by the *red points*. Filled symbols are exclusively based on SHIPTRAP data [15, 112]

benchmark for nuclear models that are used to describe superheavy elements and can thus be used to improve predictions of the island of stability.

7.6 Conclusions

PTMS has proven to be a versatile method that provides mass values of unprecedented accuracy even for radionuclides with short half-lives and with production rates as low as a few particles per second. Since the installation of the first Penning trap at a radioactive beam facility almost 30 years ago a new era in precision mass spectrometry has begun and resulted in many exciting scientific results contributing to great discoveries in various disciplines. Penning traps dominate the landscape in mass spectrometry to date and with ongoing and future devolvements they will advance further towards higher precision, higher selectivity, and higher sensitivity. This will pave the way to extend the reach to more exotic nuclides and lead to new breakthroughs in physics.

References

1. K. Blaum, High-accuracy mass spectrometry with stored ions. Phys. Rep. **425**, 1 (2006)
2. D. Lunney, J.M. Pearson, C. Thibault, Recent trends in the determination of nuclear masses. Rev. Mod. Phys. **75**, 1021 (2003)
3. S. Rainville, J.K. Thompson, D.E. Pritchard, An ion balance for ultra-high-precision atomic mass measurements. Science **303**, 334 (2004)
4. R.S. Van Dyck Jr., S.L. Zafonte, S. Van Liew, D.B. Pinegar, P.B. Schwinberg, Ultraprecise atomic mass measurement of the α particle and^4 He. Phys. Rev. Lett. **92**, 220802 (2004)
5. W. Shi, M. Redshaw, E.G. Myers, Atomic masses of ^{32,33}S, ^{84,86}Kr, and ^{129,132}Xe with uncertainties below 0.1 ppb. Phys. Rev. A **72**, 022510 (2005)
6. G. Gabrielse et al., Precision mass spectroscopy of the antiproton and proton using simultaneously trapped particles. Phys. Rev. Lett. **82**, 3198 (1999)

7. I.S. Towner, J. Hardy, The evaluation of V_{ud} and its impact on the unitarity of the Cabibbo-Kobayash-i-Maskawa quark-mixing matrix. Rep. Prog. Phys. **73**, 046301 (2010)
8. J. Britz, A. Pape, M.S. Antony, Coefficients of the isobaric mass equation and their correlations with various nuclear parameters. At. Data Nucl. Data Tables **69**, 125 (1998)
9. W. Heisenberg, Über den Bau der Atomkerne. Z. Phys. **77**, 1 (1932)
10. E.P. Wigner, in *Proceedings of the Robert A. Welch Conferences on Chemical Research*, vol 1 (Robert A. Welch Foundation, Houston, 1957), p. 67
11. O. Sorlin, M.-G. Porquet, Evolution of the N = 28 shell closure: a test bench for nuclear forces. Physica Scripta **T152**, 014003 (2013)
12. I. Tanihata, H. Savajols, R. Kanungo, Recent experimental progress in nuclear halo structure studies. Prog. Part. Nucl. Phys. **68**, 215 (2013)
13. W. Noertershaeuser, T. Neff, R. Sanchez, I. Sick, Charge radii and ground state structure of lithium isotopes: Experiment and theory reexamined. Phys. Rev. C **84**, 024307 (2011)
14. Z. Patyk, A. Sobiczewski, Ground-state properties of the heaviest nuclei analyzed in a multidimensional deformation space. Nucl. Phys. A **533**, 132 (1991)
15. E. Minaya Ramirez et al., Direct mapping of nuclear shell effects in the heaviest elements. Science **337**, 1207 (2012)
16. M. Thoennessen, Reaching the limits of nuclear stability. Rep. Prog. Phys. **67**, 1187 (2004)
17. M. Pfützner, M. Karny, L.V. Grigorenko, K. Riisager, Radioactive decays at limits of nuclear stability. Rev. Mod. Phys. **84**, 567 (2012)
18. R.G. Lovas, R.J. Liotta, A. Insolia, K. Varga, D.S. Delion, Microscopic theory of cluster radioactivity. Phys. Rep. **294**, 265 (1998)
19. H. Schatz, The importance of nuclear masses in the astrophysical rp-process. Int. J. Mass Spectrom. **251**, 293 (2006)
20. H. Schatz et al., rp-process nucleosynthesis at extreme temperature and density conditions. Phys. Rep. **294**, 167 (1998)
21. F.-K. Thielemann et al., Operation of the r-process and cosmochronology. Phys. Rep. **227**, 269 (1993)
22. F. Käppeler, The origin of the heavy elements: The s process. Prog. Part. Nucl. Phys. **43**, 419 (1999)
23. S.A. Eliseev, YuN Novikov, K. Blaum, Search for resonant enhancement of neutrinoless double-electron capture by high-precision Penning-trap mass spectrometry. J. Phys. G **39**, 124003 (2012)
24. J.J. Gomez-Cadenas, J. Martin-Albo, M. Mezzetto, F. Monrabal, M. Sore, The search for neutrinoless double beta decay. Riv. Nuovo Cim. **35**, 29 (2012)
25. J. Wolf for the KATRIN collaboratio, The KATRIN neutrino mass experiment. Nucl. Instrum. Meth. A **623**, 442 (2010)
26. G. Audi et al., The AME 2012 atomic mass evaluation. Chin. Phys. C **36**(12), 1603–2014 (2012)
27. G. Audi, The history of nuclidic masses and of their evaluation. Int. J. Mass Spectrom. **251**, 85 (2006)
28. J.J. Thomson, Cathode rays. Phil. Mag. **3**, 293 (1897)
29. J.J. Thomson, On the masses of the ions in gases at low pressures. Phil. Mag. **5**, 547 (1899)
30. J.J. Thomson, On rays of positive electricity. Phil. Mag. **13**, 561 (1907)
31. J.J. Thomson, Further experiments on positive rays. Phil. Mag. **24**, 209 (1912)
32. J.J. Thomson, Multiply-Charged atoms. Phil. Mag. **24**, 668 (1912)
33. F.W. Aston, *Mass Spectra and Isotopes*, 2nd edn. (Edward Arnold and Co., London, 1942)
34. A.J. Dempster, The energy content of the heavy nuclei. Phys. Rev. **53**, 869 (1938)
35. J. Mattauch, A double-focusing mass spectrograph and the masses of N15 and O18. Phys. Rev. **50**, 617 (1936)
36. R. Klapisch, R. Prieels, C. Thibault, A.M. Poskanzer, C. Rigaud, E. Roeckl, On-line mass-spectrometric measurement of the masses of neutron-rich sodium isotopes. Phys. Rev. Lett. **31**, 118 (1973)
37. E. Kugler, The ISOLDE facility. Hyperfine Int. **129**, 23 (2000)

38. L.G. Smith, C.C. Damm, Mass synchrometer. Rev. Sci. Instr. **27**, 638 (1956)
39. D. Lunney, D. Vieira, G. Audi et al., Mass measurements of the shortest-lived nuclides a la MISTRAL. Int. J. Mass Spectrom. **251**, 286 (2006)
40. C. Gaulard, C. Bachelet, G. Audi et al., Mass measurements of the exotic nuclides ^{11}Li and ^{11,12}Be performed with the Mistral spectrometer. Nucl. Phys. A **826**, 1 (2009)
41. G. Gärtner, E. Klempt, A direct determination of the proton-electron mass ratio. Z. Physik A **287**, 1 (1978)
42. G. Bollen, P. Dabkiewicz, P. Egelhof, T. Hilberath, H. Kalinowsky, F. Kern, H. Schnatz, L. Schweikhard, H. Stolzenberg, R.B. Moore, H.-J. Kluge, G.M. Temmer, G. Ulm,and the ISOLDE Collaboration, First absolute mass measurements of short-lived isotopes. Hyperfine Interact. **38**, 793 (1987)
43. M. Mukherjee, D. Beck, K. Blaum, G. Bollen, J. Dilling, S. George, F. Herfurth, A. Herlert, A. Kellerbauer, H.-J. Kluge, S. Schwarz, L. Schweikhard, C. Yazidjian, ISOLTRAP: An on-line Penning trap for mass spectrometry on short-lived nuclides. Eur. Phys. J. A **35**, 1 (2008)
44. M. Smith et al., First Penning-trap mass measurement of the exotic Halo nucleus ^{11}Li. Phys. Rev. Lett. **101**, 202501 (2008)
45. R. Ringle et al., High-precision Penning trap mass measurements of ^{37,38}Ca and their contributions to conserved vector current and isobaric mass multiplet equation. Phys. Rev. C **75**, 055503 (2007)
46. J. Clark et al., Improvements in the injection system of the Canadian Penning trap mass spectrometer. Nucl. Instrum. Methods B **204**, 487 (2003)
47. T. Eronen et al., JYFLTRAP: a Penning trap for precision mass spectroscopy and isobaric purification. Eur. Phys. J. A **48**, 46 (2012)
48. M. Block et al., Towards direct mass measurements of nobelium at SHIPTRAP. Eur. Phys. J. D **45**, 39 (2007)
49. G. Bollen et al., Beam cooling at the low-energy-beam and ion-trap facility at NSCL/MSU. Nucl. Instrum. Methods A **532**, 203 (2004)
50. J. Dilling et al., Mass measurements on highly charged radioactive ions, a new approach to high precision with TITAN. Int. J. Mass. Spectrom. **251**, 198 (2006)
51. J. Ketelaer et al., TRIGA-SPEC: A setup for mass spectrometry and laser spectroscopy at the research reactor TRIGA Mainz. Nucl. Instrum. Meth. A **594**, 162 (2008)
52. V.S. Kolhinen et al., MLLTRAP: A Penning trap facility for high-accuracy mass measurements. Nucl. Instrum. Meth. B **266**, 4547 (2008)
53. D. Rodriguez et al., MATS and LaSpec: High-precision experiments using ion traps and lasers at FAIR. Eur. Phys. J. ST **183**, 1 (2010)
54. A.E. Cameron, D.F. Eggers Jr, An ion 'velocitron'. Rev. Sci. Instr. **19**, 605 (1948)
55. W.R. Plass et al., Isobar separation by time-of-flight mass spectrometry for low-energy radioactive ion beam facilities. Nucl. Instrum. Meth. B **266**, 4560 (2008)
56. P. Schury et al., Multi-reflection time-of-flight mass spectrograph for short-lived radioactive ions. Eur. Phys. J. A **42**, 343 (2009)
57. R. Wolf et al., A multi-reflection time-of-flight mass separator for isobaric purification of radioactive ion beams. Hyperfine Int. **199**, 115 (2011)
58. R. Wolf et al., On-line separation of short-lived nuclei by a multi-reflection time-of-flight device. Nucl. Instrum. Meth. A **686**, 82 (2012)
59. B. Franzke, The heavy ion storage and cooler ring project ESR at GSI. Nucl. Instrum. Meth. B **24/25**, 18–25 (1987)
60. B. Franzke, H. Geissel, G. Münzenberg, Mass and lifetime measurements of exotic nuclei in storage rings. Mass Spectrom. Rev. **27**, 428 (2008)
61. YuA Litvinov, H. Geissel, R. Knöbel, B. Sun, H. Xu, Direct Mass Measurements of Exotic Nuclei in Storage Rings. Acta Physica Polonica B **41**, 511 (2010)
62. U. Koester, Intense radioactive-ion beams produced with the ISOL method. Eur. Phys. J. A **15**, 255 (2002)
63. V.N. Fedoseyev, G. Huber, U. Koster, J. Lettry, V.I. Mishin, H. Ravn, V. Sebastian, The ISOLDE laser ion source for exotic nuclei. Hyperfine Int. **127**, 409 (2000)

64. M. Huyse, R. Raabe, Radioactive ion beam physics at the cyclotron research centre Louvain-la-Neuve. J. Phys. G **38**, 024001 (2011)
65. P.G. Bricault, M. Dombsky, P.W. Schmor, G. Stanford, Radioactive ion beams facility at TRIUMF. Nucl. Instrum. Meth. B **126**, 231 (1997)
66. A. Navin, F. de Oliveira Santos, P. Roussel-Chomaz, O. Sorlin, Nuclear structure and reaction studies at SPIRAL. J. Phys. G **38**, 024004 (2011)
67. J. Arje et al., The ion guide isotope separator on-line, IGISOL. Nucl. Instrum. Meth. A **247**, 431 (1986)
68. J. Äystö, T. Eronen, A. Jokinen, A. Kankainen, I.D. Moore, H. Penttilä(eds.), An IGISOL Portrait—selected contributions. Eur. Phys. J. A **48** (2012)
69. H. Sakurai, RI beam factory project at RIKEN. Nucl. Phys. A **805**, 526c (2008)
70. H. Geissel et al., The GSI projectile fragment separator (FRS): a versatile magnetic system for relativistic heavy ions. Nucl. Instrum. Meth. B **70**, 286 (1992)
71. D.J. Morrissey, B.M. Sherrill, M. Steiner, A. Stolz, I. Wiedenhöver, Commissioning the A1900 projectile fragment separator. Nucl. Instrum. Meth. B **204**, 90 (2003)
72. S. Hofmann, G. Münzenberg, The discovery of the heaviest elements. Rev. Mod. Phys. **72**, 733 (2000)
73. A.V. Yeremin, The kinematic separator VASSILISSA performance and experimental results. Nucl. Instrum. Meth. A **350**, 608 (1994)
74. Yu. Ts, Oganessian, Heaviest nuclei from ^{48}Ca-induced reactions. J. Phys. G **34**, R165 (2007)
75. V. Ninov, K.E. Gregorich, C.A. McGrath, The Berkeley Gas-filled separator. AIP Conf. Proc. **455**, 704 (1998)
76. K. Morita et al., RIKEN isotope separator on-line GARIS/IGISOL. Nucl. Instrum. Meth. B **70**, 220 (1992)
77. M. Leino et al., Gas-filled recoil separator for studies of heavy elements. Nucl. Instrum. Meth. B **99**, 653 (1995)
78. A. Semchenkov et al., The TransActinide separator and chemistry apparatus (TASCA) at GSI optimization of ion-optical structures and magnet designs. Nucl. Instrum. Meth. B **266**, 4153 (2008)
79. G. Savard, St Becker, G. Bollen, H.-J. Kluge, R.B. Moore, L. Schweikhard, H. Stolzenberg, U. Wiess, A new cooling technique for heavy ions in a Penning trap. Phys. Lett. A **158**, 247–252 (1991)
80. C.N. Davids, D. Peterson, A compact high-resolution isobar separator for the CARIBU project. Nucl. Instrum. Meth. B **266**, 4449 (2008)
81. F. Herfurth, Segmented linear RFQ traps for nuclear physics. Nucl. Instrum. Meth. B **204**, 587 (2008)
82. G. Savard et al., Large radio-frequency gas catchers and the production of radioactive nuclear beams. J. Phys. Conf. Ser. **312**, 052004 (2011)
83. M. Wada et al., Slow RI-beams from projectile fragment separators. Nucl. Instrum. Meth. B **204**, 570 (2003)
84. L. Weissman et al., First extraction tests of the NSCL gas cell. Nucl. Phys. A **746**, 655 (2004)
85. J.B. Neumayr et al., The ion-catcher device for SHIPTRAP. Nucl. Inst. Meth. B **244**, 489 (2005)
86. Yu. Kudryavtsev et al., Dual chamber laser ion source at LISOL. Nucl. Inst. Meth. B **267**, 2908 (2009)
87. S. Schwarz, RF ion carpets: the electric field, the effective potential, operational parameters and an analysis of stability. Int. J. Mass Spectrom. **299**, 71 (2011)
88. M. Ranjan et al., New stopping cell capabilities: RF carpet performance at high gas density and cryogenic operation. Europhys. Lett. **96**, 52001 (2011)
89. C. Droese et al., GSI Scientific Report 2012
90. I. Katayama et al., Cyclotron ion guide for energetic radioactive nuclear ions. Hyperfine Int. **115**, 165 (1998)
91. G. Bollen, D.J. Morrissey, S. Schwarz, A study of gas-stopping of intense energetic rare isotope beams. Nucl. Inst. Meth. A **550**, 27 (2005)

92. G. Bollen et al., Efficient and fast thermalization of Rare Isotope Beam from projectile fragmentation. The cyclotron gas stopper project at the NSCL. Eur. Phys. J. Spec. Top. **150**, 265 (2007)
93. F. Herfurth, A linear radiofrequency ion trap for accumulation, bunching, and emittance improvement of radioactive ion beams. Nucl. Instrum. Meth. A **469**, 254 (2001)
94. A. Nieminen et al., Beam cooler for low-energy radioactive ions. Nucl. Instrum. Meth. A **469**, 244 (2001)
95. S. Schwarz et al., A second-generation ion beam buncher and cooler. Nucl. Instrum. Meth. B **204**, 474 (2003)
96. F. Major, V.N. Gheorghe, G. Werth, *Charged Particle Traps— Physics and Techniques of Charged Particle Field Confinement*, 1st edn. (Springer, Heidelberg, 2005)
97. G. Werth, V.N. Gheorghe, F.G. Major, *Charged Particle Traps II* (Springer, Heidelberg, 2009)
98. P.H. Dawson, *Quadrupole Mass Spectrometry and Its Applications* (Elsevier, Amsterdam, 1995)
99. P. Ghosh, *Ion Traps* (Oxford University Press, Oxford, 1995)
100. W. Paul, Electromagnetic traps for charged and neutral particles. Rev. Mod. Phys. **62**, 531 (1990)
101. H.G. Dehmelt, Experiments with an isolated subatomic particle at rest. Rev. Mod. Phys. **62**, 525 (1990)
102. L.S. Brown, G. Gabrielse, Geonium theory: Physics of a single electron or ion in a Penning trap. Rev. Mod. Phys. **58**, 233 (1986)
103. M. Kretzschmar, Int. J. Mass Spectrom., submitted (2013)
104. G. Bollen et al., The accuracy of heavy-ion mass measurements using time of flight-ion cyclotron resonance in a Penning trap. J. Appl. Phys. **68**, 4355 (1990)
105. L. Schweikhard, G. Bollen (eds.). Int. J. Mass Spectrom. 251 (2006)
106. F.M. Penning, Verzögerungen bei der Zündung von gasgefüllten Photozellen im Dunkeln. Physica **3**, 563 (1936)
107. J.R. Pierce, *Theory and Design of Electron Beams* (D. van Nostrand Co., NewYork, 1949). (Chapter 3)
108. S. George et al., The Ramsey method in high-precision mass spectrometry with Penning traps: experimental results. Int. J. Mass Spectrom. **264**, 110 (2007)
109. G. Gräff, H. Kalinowsky, J. Traut, A direct determination of the proton electron mass ratio. Z. Physik A **297**, 35 (1980)
110. M. König, G. Bollen, H.-J. Kluge, T. Otto, J. Szerypo, Quadrupole excitation of stored ion motion at the true cyclotron frequency. Int. J. Mass Spec. Ion Proc. **142**, 95 (1995)
111. G. Gabrielse, The true cyclotron frequency for particles and ions in a Penning trap. Int. J. Mass Spectrom. **279**, 107 (2009)
112. M. Block, Direct mass measurements above uranium bridge the gap to the island of stability. Nature **463**, 785 (2010)
113. A. Kellerbauer, Recent improvements of ISOLTRAP: absolute mass measurements of exotic nuclides at 10^{-8} precision. Int. J. Mass Spectr. **229**, 107 (2003)
114. G. Bollen, Mass measurements of short-lived nuclides with ion traps. Nucl. Phys. A **693**, 3 (2001)
115. S. Eliseev et al., Octupolar excitation of ions stored in a Penning trap mass spectrometerA study performed at SHIPTRAP. Int. J. Mass Spectrom. **262**, 45 (2007)
116. R. Ringle et al., Octupolar excitation of ion motion zin a Penning trapA study performed at LEBIT. Int. J. Mass Spectrom. **262**, 33 (2007)
117. S. Eliseev et al., Octupolar-excitation Penning-trap mass spectrometry for Q-value measurement of double-electron capture in 164Er. Phys. Rev. Lett. **107**, 152501 (2011)
118. S. Ettenauer et al., First use of high charge states for mass measurements of short-lived letN=Y nuclides in a Penning trap. Phys. Rev. Lett. **107**, 272501 (2012)
119. S. Eliseev et al., Phase-Imaging Ion-Cyclotron-Resonance measurements for short-lived nuclides. Phys. Rev. Lett. **110**, 082501 (2013)

120. A. Kellerbauer et al., From direct to absolute mass measurements: a study of the accuracy of ISOLTRAP. Eur. Phys. J. D **22**, 53 (2003)
121. M. Block et al., Towards direct mass measurements of nobelium at SHIPTRAP. Eur. Phys J. D **45**, 39 (2007)
122. C. Droese et al., Investigation of the magnetic field fluctuation and implementation of a temperature and pressure stabilization at SHIPTRAP. Nucl. Instrum. Meth. A **632**, 157 (2011)
123. G. Gabrielse, F.C. Mackintosh, Cylindrical Penning traps with orthogonalized anharmonicity compensation. Int. J. Mass Spec. Ion Proc. **57**, 1 (1984)
124. G. Bollen et al., Resolution of nuclear ground and isomeric states by a Penning trap mass spectrometer. Phys. Rev. C **46**, R2140 (1992)
125. C. Fröhlich et al., Composition of the innermost core-collapse Supernova Ejecta. Ap. J. **637**, 415 (2006)
126. T. Beier, The status of FAIR. Hyperfine Int. **194**, 99 (2009)
127. G. Bollen, FRIBFacility for rare isotope beams. AIP conf. proc. **1224**, 432 (2010)
128. . M. Lewitowicz, Status of the SPIRAL2 Project. Acta Physica Polonica B **42**, 877 (2011)
129. S. Wanajo, S. Goriely, M. Samyn, N. Itoh, The r-Process in Supernovae: impact of new microscopic mass formulae. Ap. J. **606**, 1057 (2004)
130. A. Arcones, G.F. Bertsch, Nuclear Correlations and the r Process. Phys. Rev. Lett. **108**, 151101 (2012)
131. J. Savory et al., Nuclear Scission and Quantum Localization. Phys. Rev. Lett. **107**, 132501 (2009)
132. A. Martín et al., Mass measurements of neutron-deficient radionuclides near the end-point of the rp-process with SHIPTRAP. Eur. Phys. A **34**, 341 (2007)
133. P. Schury et al., Precision mass measurements of rare isotopes near N=Z=33 produced by fast beam fragmentation. Phys. Rev. C **75**, 055801 (2007)
134. C. Weber et al., Mass measurements in the vicinity of the r p-process and the p-process paths with the Penning trap facilities JYFLTRAP and SHIPTRAP. Phys. Rev. C **78**, 054310 (2008)
135. E. Haettner et al., Mass measurements of very Neutron-Deficient Mo and Tc isotopes and their impact on rp Process Nucleosynthesis. Phys. Rev. Lett. **106**, 122501 (2011)
136. J. Fallis et al., Mass measurements of isotopes of Nb, Mo, Tc, Ru, and Rh along the vp- and rp-process paths using the Canadian Penning trap mass spectrometer. Phys. Rev. C **84**, 045807 (2011)
137. A. Kankainen et al., Isomer and decay studies for the rp process at IGISOL. Eur. Phys. J. A **48**, 49 (2012)
138. J. Van Schelt et al., Mass measurements near the r-process path using the Canadian Penning Trap mass spectrometer. Phys. Rev. C **85**, 045805 (2012)
139. R. Wolf et al., Plumbing neutron stars to new depths with the binding energy of the exotic nuclide ^{82}Zn. Phys. Rev. Lett. **110**, 041101 (2013)
140. M. Bender et al., Shell structure of superheavy nuclei in self-consistent mean-field models. Phys. Rev. C **60**, 034304 (1999)
141. S. Cwiok et al., Shape coexistence and triaxiality in the superheavy nuclei. Nature **433**, 705 (2005)
142. P. Møller, J.R. Nix, Nuclear ground-state masses and deformations. At. Data Nucl. Data Tab. **59**, 185 (1995)
143. L. Stavsetra et al., Independent verification of element 114 production in the ^{48}Ca + ^{242}Pu reaction. Phys. Rev. Lett. **103**, 132502 (2009)
144. ChE Düllmann et al., Production and decay of element 114: High cross sections and the new nucleus ^{277}Hs. Phys. Rev. Lett. **104**, 252701 (2010)
145. S. Hofmann et al., The reaction ^{48}Ca + ^{248}Cm $\rightarrow$ 296,116* studied at the GSI-SHIP. Eur. Phys. J. A **48**, 62 (2012)
146. K. Morita et al., New result in the production and decay of an isotope, ^{278}113, of the 113th element. J. Phys. Soc. Jpn. **81**, 103201 (2012)
147. Yu.Ts. Oganessian et al., Synthesis of the heaviest elements in ^{48}Ca-induced reactions, Radiochim. Acta **99**, 429 (2011)